Tool to predict and avoid Partial Discharges in stator slot of rotating motors fed by inverter

Philippe Collin, David Malec, Yvan Lefèvre

Tool to predict and avoid Partial Discharges in stator slot of rotating motors fed by inverter

Philippe COLLIN, David MALEC, Yvan LEFEVRE

LAPLACE, Université de Toulouse, CNRS, INPT, UPS, France

118, route de Narbonne - bât 3R3 - 31062 Toulouse cedex 9

collin@laplace.univ-tlse.fr

KEYWORDS: partial discharges, parametric models, motorette, electric motor, Paschen.

ABSTRACT:

The introduction of power electronics opened a wide range of possibilities in machines control. However, fast switching frequencies of the converters combined with the power cable length lead to repetitive transient overshoots on the motor terminals. They do not spread linearly across the motor winding. The first turns, which are closest to the terminals, are the most impacted. High transient electric field occurs in the slot which may ignite partial discharges (PD) and accelerate the motor electric insulation aging. This paper presents a tool to detect and avoid PD in the stator slot of low voltage rotating motors fed by inverter. The context is a more electric aircraft. First, it will briefly introduce the challenges toward a hybrid propelled aircraft. Then some generalities concerning low voltage rotating machines insulation and PD will be presented. Parametric models for the evaluation of the partial discharge insulation voltage (PDIV) are obtained from 2D finite elements models. These are used in a tool to predict PD risk in a motorette.

1. Introduction

In the context of energy transition, more electric transportation is a key challenge. Hybrid and full electric automotives are proposed by more and more car manufacturers. The main motivation is environmental. It aims to be compliant with European targets on the reduction of CO_2 emission in the transports industry. This tendency also targets the aeronautic industry. Future aircrafts have to consume less fuel and produce less noise. The future technologies are being studied by the European Clean Sky 2 consortium.

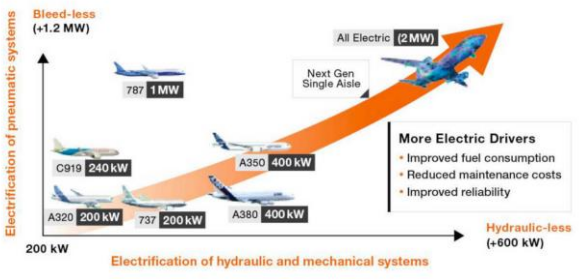

Figure 1. Increasing onboard electrical equipment demand in commercial aviation [1]

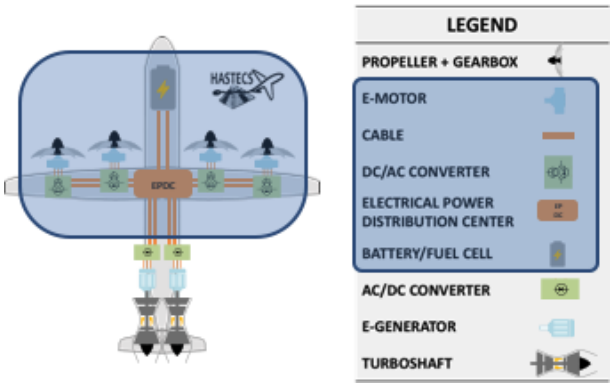

Figure 2. Serial hybrid powertrain [2]

The electrification of planes presents many advantages: improved fuel consumption, reduced maintenance costs and improved reliability. Fig. 1 illustrates the increase of in board electric power compare to the reduction of traditional pneumatic power.

The HASTECS project focuses on a serial hybrid electric propelled aircraft powertrain. It is shown on Fig. 2. A gas turbine powers an electric generator. The electric power is provided by this generator and additional batteries. A DC bus routes the power from the sources to the motors located in the nacelles. It is converted from DC to AC via inverters. The first target to be reached in 2025 is to get a *5kW/kg* electric motor (cooling system included) without any partial discharges (PD). To reach such high-power density the velocity, and thus the voltage, have to be increased. DC voltage bus will overpass *1kV*. In recent aircraft such as Boeing 780 and Airbus A380 and A350, the voltage is regulated at either *115* or *230Vac* [3]. The rise of the onboard voltage represents a real challenge for the safety of both the passengers and the systems.

The whole powertrain is optimized in order to minimize embedded weight and maximize the power efficiency [4]. In this paper the focus is made on the electric motor. The motor is sized using a developed design tool [5]. The sensitivity of the thermal behavior is investigated in order to provide a cooling solution [6]. Besides, due to the increased voltage level and risk of overshoots at the motor terminals, PD risk has to be dealt with from the design step. Ultimately, the optimization of the motor alone has to consider the electromechanical, thermal and electrical constraints.

The work presented in this paper is about the primary electrical insulation system of high-power density electric machine. Because of poor thermal properties of electric insulation materials, there is an important coupling between the thermal sizing and the PD free sizing for the challenging application of hybrid propelled aircraft.

2. Low voltage rotating motor electric insulation

There are two kinds of materials having good electrical insulation properties: the organic (polymers) and non-organic (ceramics) materials. Due to the vibrations, the electric insulation of onboard motor is mainly composed of polymers. This paper focuses on low voltage rotating machine, i.e phase to phase voltage lower than *700Vrms*. The primary electrical insulation on the stator of these machines is multilayers as shown on Fig. 3. In this work, it is considered to have only *1* phase per slot. The PD risk zones are then reduced to turn to turn and turn to ground insulation. The choice of the insulation materials is determined by the environmental constrains applied on the motor, mainly the temperature and the humidity. The insulation power of polymers is highly affected by the temperature. These materials are distributed into thermal classes which define the highest temperature at which they are able to assure their insulation function. Some thermal classes are presented on Tab. 1.
Generally, the slot is filled with an Epoxy resin. It fixes the winding in the slot and improves the thermal conductivity compared to air. However, thermal properties of classic polymer materials are quite bad. Thermal conductivities are around *0.14-1W/m.K* [7]. It is over *80* times lower than the one of iron (*80W/m.K*).
The dielectric strength of polymers are located around *14-30kV/mm* [7]. It can be more than 10 times the one of dry air (*3kV/mm*). A polymer has a dielectric constant bigger than *1*, which value corresponds to dry air.

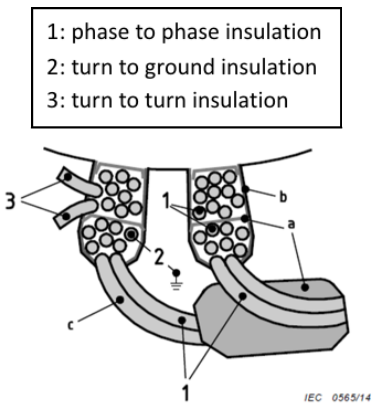

Figure 3. Main electrical insulation on a stator slot of low voltage machine -a)phase separator, b)slot insulation, c)enamel overcoat [8]

Table 1. Some thermal classes [9]

Thermal class	F	H	N	-	-	-
Temperature (°C)	155	180	200	220	250	280

It explains why it possesses such good dielectric strength. Common values for dielectric constants are around *2-6*. The common tendency is the biggest the dielectric constant, the lowest electric field intensity you get in the dielectric and the biggest intensity you get outside the dielectric.
In this paper, a non-impregnated slot is considered for the numerical simulations. Other work has shown that, for an impregnated twisted pair, the results obtained experimentally are close to the ones obtained by simulation with a non-impregnated configuration [10]. This can be explained by the hypothesis done in simulations, such as the lack of air bubbles in the insulation. This observation is extrapolated to the case of a stator slot.

3. Partial discharge (PD) evaluation

The Paschen's criterion is widely used in the literature for the prediction of PD in numerical models [10],[11],[12]. To apply it, one needs to know precisely the field lines geometry and the associated voltage drop. Besides, the following hypothesis have to be checked:

1) the discharge takes place in the air
2) the electric field in the PD risk zone is uniform

The mechanism behind this criterion is the electronic avalanche [10], [11]. An important phenomenon is the injection of electrons in the air gap due to ions impacting the cathode. This secondary electron emission in the air gap is characterized by the second Townsend's coefficient. It is the ratio of the number of ejected electrons in the gap participating to the avalanche over the number of impacting ions on the cathode. This coefficient strongly depends on the nature and the geometry of the electrodes. It highly impacts the partial discharge insulation voltage (PDIV) level. In the literature, a value of this coefficient for metallic planar electrodes is *0.01* [13]. Experiments have been conducted in another work to correct this value with a configuration of two enameled round wires in close contact. An averaged corrected value of *9e-4* is extracted [14]. Fig. 4 illustrates the use of Paschen's curve in the prediction of PD considering 2 enameled round wires in close contact.

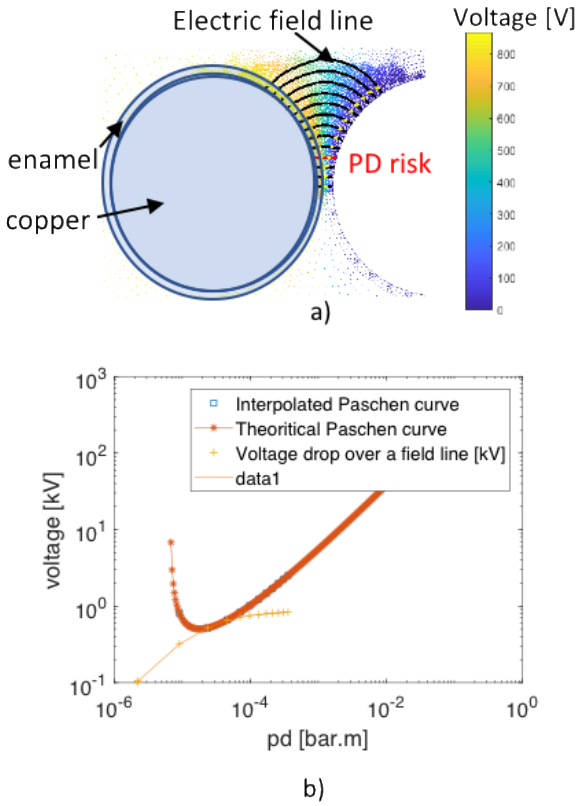

Figure 4. a) Electric field lines and PD risk field line (red); b) Voltage drops across field lines as a function of product pressure (1bar) time field lines length in air gap (d) – comparison with Paschen's curve with second Townsend's coefficient of 5e-4 [14]

The field line in red (Fig. 4.a) may contain PD. The corresponding point on Fig. 4.b intersects the Paschen's curve (red curve).

4. Partial discharge insulation voltage (PDIV) parametric models

The work presented in this paper has been carried out under normal conditions of pressure and temperature (i.e at *20°C* and *1bar*). Thus, the required voltage drop to initiate a discharge mainly depend on the geometric configuration and the material properties. In this paper, the conductors are considered as copper round wires overcoated with a uniform polymer layer. The slot insulation is chosen composed of *2* insulation layers of same thickness. These layers can be formed of different materials. Due to symmetries and invariance along the motor active length (***z*** axis), reduced 2D finite elements models are used. They are shown on Fig. 5. They are computed with the commercial software *Ansys Mechanical APDL*. Voltage potentials are applied on the inner wire radius. The machine slot is grounded. A tangential field boundary conditions is applied by default on the limits of the domain. The dielectric constant of the polymer overcoating the wires is taken equals to *3.5*. It is a common value for polymers used to constitute the enamel layer. The secondary

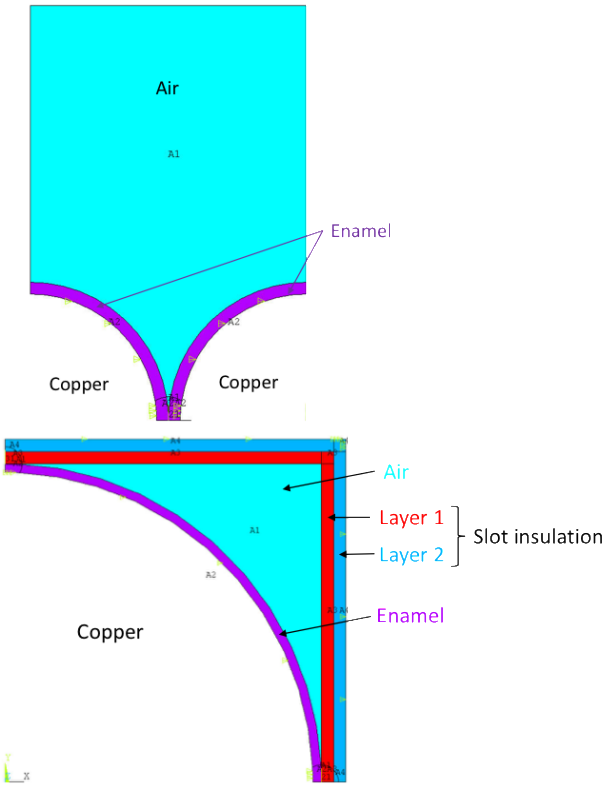

Figure 5. Top) turn to turn reduced model; below) turn to slot reduced model – slot insulation composed of 2 layers of same thickness

electron emission coefficients in Paschen's curve calculation is taken equals to *9e-4* according to [14].

Tab. 2 presents the geometric and material parameters used in the parametric study. It can be seen that the turn to slot parametric study is by far the most complex. In this paper, the number of slot insulation layers is fixed to *2*. However, in some cases it can reach *4* layers. This would increase the number of cases to study the impact of the superposition of different material layers on PDIV level. Besides, the *2* layers have the same thickness. A much more complex study is required to study the impact of non-homogenous slot insulation layers on PDIV.

The objective is to derived simple mathematical laws of the evolution of PDIV as a function of the presented parameters from the 2D finite elements models. These computed laws are confronted to a simple analytical model to check the results.

The analytical model is a very simplified vision of the problem. The electric field lines in this model are approximated to straight line. The lines length in the gap between *2* round conductors is determined using geometric relations as in [11]. The field line is delimited with a tube. The tube is considered thin enough so that the materials are considered as planar capacitances. Fig. 6 illustrates the idea of flux tube and the resulting analytical circuit model representing the turn to turn configuration.

Table 2. Parameters used in the parametric study for turn to turn & turn to slot models

Turn to turn model	R_{int}	Wire copper radius
	e	Wire enamel overcoat thickness
	$ratio_{Geo}$	Ratio of wire geometric parameters $ratio_{Geo} = \frac{e}{R_{int}}$
	grade	Parametric grade insulation (from 0 to 1). It depicts the enamel thickness.
Turn to slot model	ε_{layer1}	Dielectric constant of layer 1 slot insulation
	ε_{layer2}	Dielectric constant of layer 2 slot insulation
	$ratio_{\varepsilon lay}$	Ratio of slot insulation layer dielectric constants $ratio_{\varepsilon lay} = \frac{\varepsilon_{layer1}}{\varepsilon_{layer2}}$
	layer	Total slot insulation thickness
	R_{int}	Wire copper radius
	e	Wire enamel overcoat thickness
	$ratio_{Geo}$	Ratio of wire geometric parameters $ratio_{Geo} = \frac{e}{R_{int}}$
	grade	Parametric grade insulation (from 0 to 1). It depicts the enamel thickness.

In the analytical model, the electric field ***E*** and electric field density ***D*** are purely normal. They are noted *E* and *D* respectively. The *D* field is conservative on the air/polymer interfaces:

$$D_{air} = D_{diel} \qquad (1)$$
$$E_{air}.\varepsilon_0 = E_{diel}.\varepsilon_0.\varepsilon_r$$

With E_{air} and E_{diel} the electric field respectively in the air gap and in the dielectric overcoating the conductors, D_{air} and D_{diel} the electric field density in the air gap and the dielectric respectively, ε_0 and ε_r the dielectric constants of vacuum and the dielectric respectively.

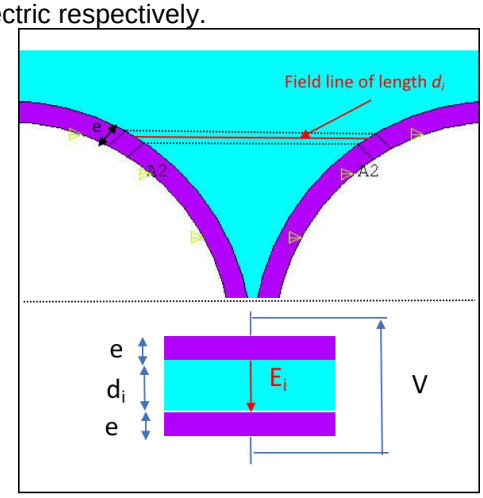

Figure 6. Top) example of straight field line and associated tube; below) resulting analytical circuit model

Based on Eq. 1 it is possible to derive the electric field in the air gap as a function of the applied voltage *V*, the geometric and dielectric parameters as in [15]:

$$E_{air} = \frac{V}{d_i + 2.e.\frac{1}{\varepsilon_r}} \qquad (2)$$

5. Turn to turn PDIV parametric model

Geometric parameters of the enameled round wires are extracted from a manufacturer brochure [16]. Copper diameters range goes from *0.18mm* to *5mm*. Three insulations grades are given. For each grade, the minimal and maximum tolerance for the enamel thickness is provided. Fig. 7 displays the evolution of PDIV as a function of $ratio_{Geo}$ as defined in Tab. 2. The plot is in logarithmic scale. For each copper diameter, the minimum and maximum tolerance values of all *3* grades has been considered.
Linear equations depending on the grade values can be extracted. A parametric axis shown on Fig. 8 is used to identify the considered grade level (i.e the selected enamel thickness). In this paper, the maximum enameled thickness is considered to be delimited by maximum *grade 3* tolerance. In future work, the grade axis will be unenclosed.
The equations in the logarithmic space have the form:

$$y=a(grade).x+b(grade) \qquad (3)$$

With *a* and *b* the coefficients which are dependent of the parametric *grade* value located between *0* and *1*.
The evolution of these coefficients as a function of *grade* is displayed on Fig. 9. As the grade axis is closed, the coefficients values are piecewise linearly interpolated.

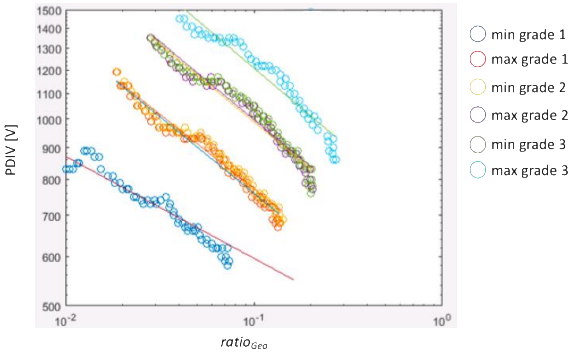

Figure 7. PDIV evolution as a function of $ratio_{Geo}$ for different enamel thicknesses

Figure 8. Grade parametric axis

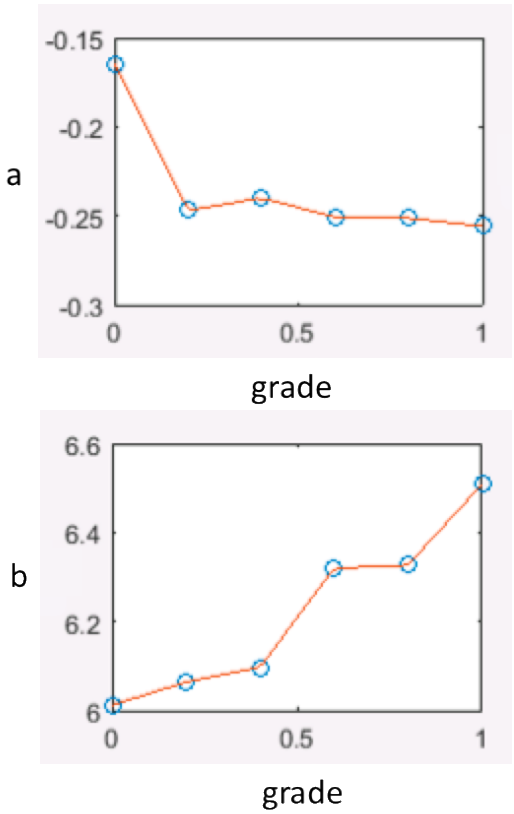

Figure 9. Linear coefficients as a function of grade

A change of variable if finally applied to express the evolution of PDIV as a function of $ratio_{Geo}$ in linear scale. It corresponds to a power law.

Linear equation	*y=a(grade).x+b(grade)*	(4)
Change of variable	$\begin{cases} PDIV = e^{y} \\ ratio_{Geo} = e^{x} \\ b' = e^{b} \end{cases}$	
Power law	$PDIV = b'(grade).ratio_{Geo}^{a(grade)}$	

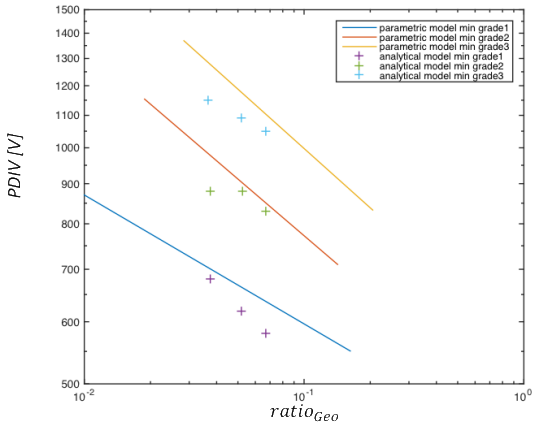

Figure 10. PDIV values from parametric model vs analytic model

Table 3. Parameters values for parametric model validation with simple analytical model

$ratio_{Geo}$	*grade*	*e*	R_{int}	PDIV parametric model	PDIV analytical model
0.0376	0	16μm	0.425 mm	700V	680V
0.0375	2/5	35 μm	0.8mm	976V	880V
0.0366	4/5	65 μm	1.775 mm	1284V	1150V
0.0518	0	11 μm	0.2125mm	664V	620V
0.0523	2/5	34.5 μm	0.66 mm	904V	880V
0.0518	4/5	58 μm	1.12 mm	1175V	1090V
0.0670	0	7.5 μm	0.112 mm	636V	580V
0.0667	2/5	30 μm	0.45 mm	851V	830V
0.0669	4/5	53.5 μm	0.8mm	1106V	1050V

The computed parametric model is then confronted to the simplified analytical model presented in paragraph 4. The verification focuses on minimal *grade 1*, *grade 2* and *grade 3* enamel thickness. Three different $ratio_{Geo}$ values are picked up. Tab. 3 recaps the parameters values used in this comparison and the obtained PDIV values.
Fig. 10 displays the PDIV results obtained with the 2 models. Values from the analytical model are represented by crosses. It can be seen that the order of magnitude of PDIV and the linear evolution of the parametric model is compliant with the analytical results.

6. Turn to slot PDIV parametric model: analytical approach

It is a more complex task to undertake this work for the wire to slot configuration. There are more parameters to account for, and consequently more variations. This time, a simple analytic model is first used to determine the impact of each parameters on PDIV. The conclusions are then validated with finite elements model.
The wire to slot analytical model is constructed on the same bases than the turn to turn analytical model presented on Fig. 6. The same assumption is applied. The only difference come from the dissymmetry of the DBD configuration due to the *2* insulation layers constituting the slot insulation.

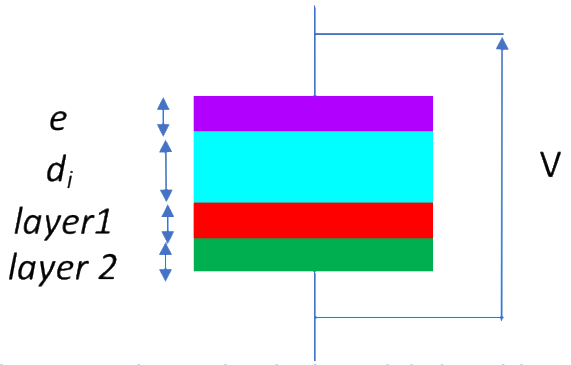

Figure 11. Wire to slot simple analytical model DBD configuration

Fig. 11 presents the DBD configuration used for the simple analytical model.
With *e* the thickness of the enamel layer around the wire, d_i the air gap length, *layer1* and *layer2* the thickness of the 2 insulation layers. Let's designate by ε_{re}, $\varepsilon_{rlayer1}$ and $\varepsilon_{rlayer2}$ the dielectric constants of the enamel, the slot insulation 1st and 2nd layer respectively.
The electric field in the air gap is expressed similarly as in (2):

$$E_{air} = \frac{V_{air}}{d_i} = \frac{V}{d_i + e * \frac{1}{\varepsilon_{re}} + layer1 * \frac{1}{\varepsilon_{rlayer1}} + layer2 * \frac{1}{\varepsilon_{rlayer2}}} \quad (4)$$

At first, the impact of *layer* parameter is investigated with the analytical model. Tab. 4 gives the parameters values. Fig. 12 presents the evolution of PDIV for ε_{layer1}=*6* as a function of slot insulation *layer*.

Table 4. Parameters values for the parametric study

ε_{layer1}, ε_{layer2}	Dielectric constant of layers 1 & 2 slot insulation	1.6 - 2.3 - 3.2 - 4.5 - 6 - 8
$ratio_{\varepsilon lay}$	Ratio of slot insulation layer dielectric constants $ratio_{\varepsilon lay} = \frac{\varepsilon_{layer1}}{\varepsilon_{layer2}}$	
layer	Total slot insulation thickness	20-40-60-100-140μm
R_{int}	Wire copper radius	0.5mm
e	Wire enamel overcoat thickness	40 μm
$ratio_{Geo}$	Ratio of wire geometric parameters $ratio_{Geo} = \frac{e}{R_{int}}$	0.08
grade	Parametric grade insulation (from 0 to 1). It depicts the enamel thickness.	2.5/5 (medium grade 2)

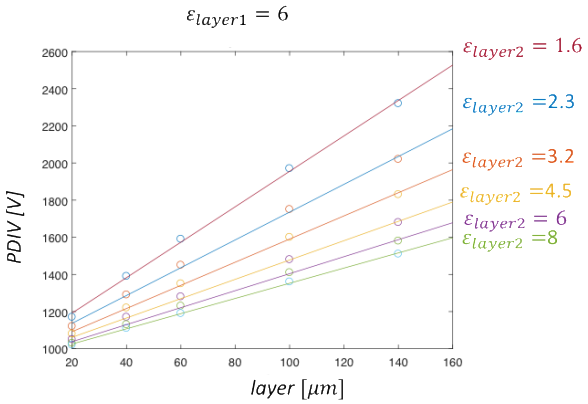

Figure 12. PDIV as a function of layer at a fixed ε_{layer1} – analytic model

The evolution is linear. The coefficients c_1 and c_2 of Eq. 4 are dependent of the slot insulation layers dielectric constants.

$$PDIV = c_1(\varepsilon_{layer1} ratio_{\varepsilon lay}) * layer + c_2(\varepsilon_{layer1} ratio_{\varepsilon lay}) \quad (4)$$

The dependency of these coefficients as a function of $ratio_{\varepsilon lay}$ for $\varepsilon_{layer1} = 6$ is presented on Fig. 13. The evolution is linear. Let's designate by *c* either c_1 or c_2 coefficients on Eq. 5.

$$c = d1(\varepsilon_{layer1}) * ratio_{\varepsilon lay} + d2(\varepsilon_{layer1}) \quad (5)$$

The evolution of d_1 and d_2 coefficients as a function of ε_{layer1} is presented on Fig. 14. The blue curved are attached to c_2, the green ones to c_1.

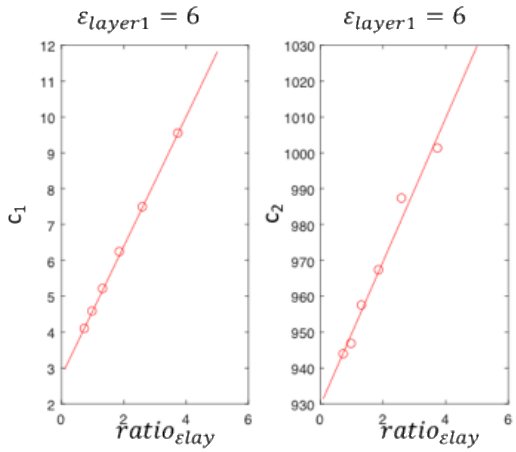

Figure 13. c coefficients linear evolution as a function of $ratio_{\varepsilon lay}$ – analytic model

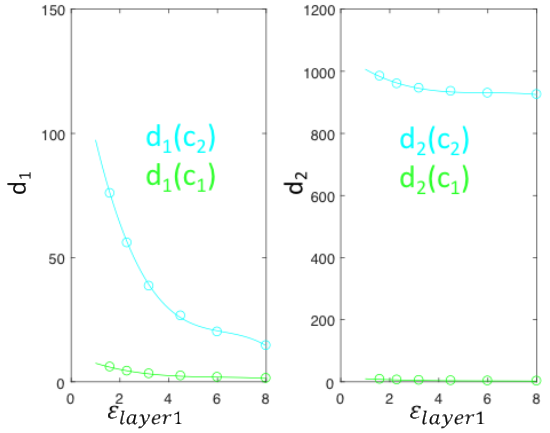

Figure 14. Evolution of d1 and d2 as a function of ε_{layer1} – analytic model

Let's designate by *d* either d_1 or d_2 coefficients. The evolution is interpolated using a 3rd order polynom:

$$d = h_1 * \varepsilon_{layer1}{}^3 + h_2 * \varepsilon_{layer1}{}^2 + h_3 * \varepsilon_{layer1} + h_4 \quad (6)$$

Let's designate by *h* either h_1, h_2, h_3 or h_4 coefficients. The evolution of *h* attached to d_1 blue curve on Fig. 14 as a function of enamel thickness *e* is presented on Fig. 15.
The dispersion of the points can be explained by the impact of the $ratio_{Geo}$ parameter. However, considering only *e* parameter results in quite a good approximation and the evolution of *h* as a function of *e* only is interpolated as a line.

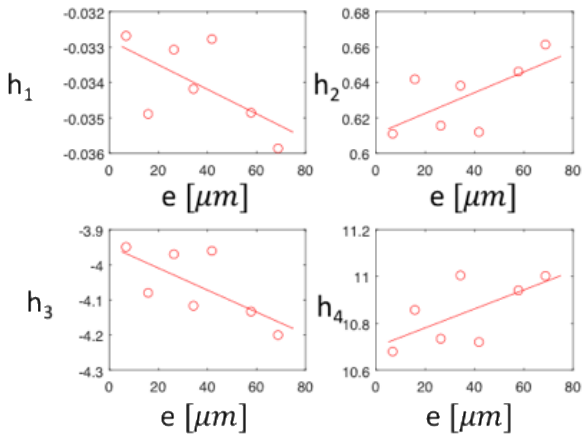

Figure 15. h coefficients attached to $d_1(c_2)$ as a function of e – analytic model

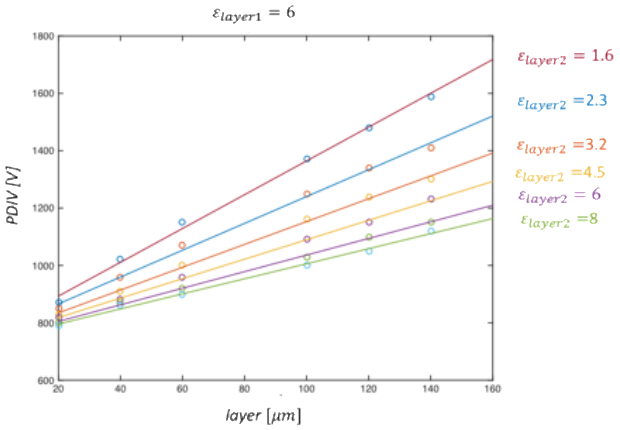

Figure 16. PDIV as a function of layer at a fixed ε_{layer1} – 2D finite elements model

7. Turn to slot parametric model: finite elements approach

The parametric model established using the simplified analytic approach is validated with a 2D finite elements model of the turn to slot configuration presented on Fig. 5. The procedure established in paragraph 6 is continued.

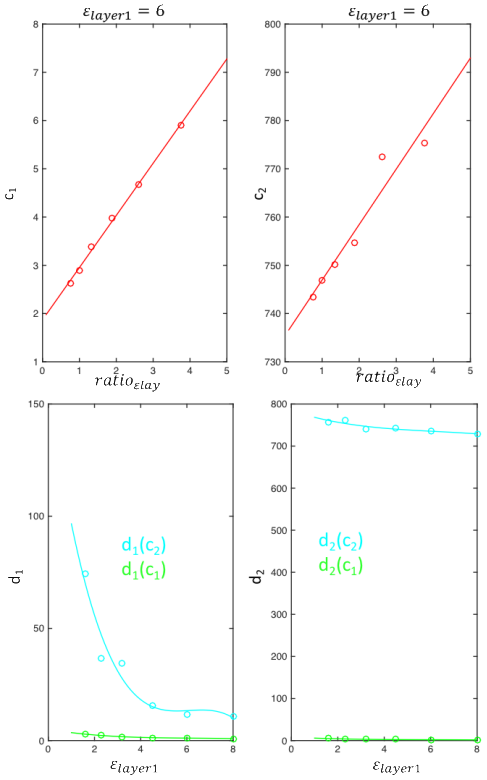

Figure 17. Top) c coefficients linear evolution as a function of $ratio_{\varepsilon lay}$;below) evolution of d1 and d2 as a function of ε_{layer1} – 2D finite elements model

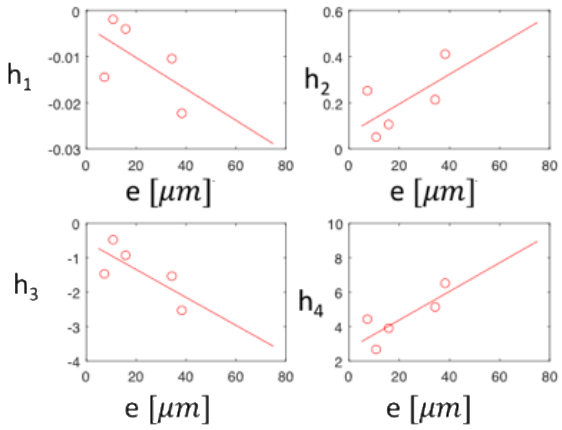

Figure 18: h coefficients attached to $d_1(c_2)$ as a function of e – 2D finite elements model

The evolution of PDIV as a function of slot insulation global layer obtained from the 2D finite elements model is displayed on Fig. 16. It follows the same kind of linear law (Eq. 5) as found with the analytic model (Fig. 12). However, the PDIV amplitudes are lower of almost a factor *2*. This can be explained by the strong hypothesis used in the simplified analytic model. The evolution of *c* and *d* coefficients are displayed on Fig. 17.
The *c* and *d* coefficients follow the linear and cubic laws established in (Eq. 5) and (Eq. 6) respectively. Finally, the evolution of *h* coefficients attached to blue curve $d_1(c_2)$ is presented on Fig. 18.
There is more dispersion but considering only the impact of *e* instead of $ratio_{Geo}$ leads to a good linear interpolation as predicted with the simplified analytical model.

8. Tool to evaluate PD risk

The finite elements based parametric models are used in a tool to help a machine designer to consider partial discharge phenomena in stator slot. The use of this tool has been introduced in [5]. In this paragraph, a motorette is considered as an illustrative example. It consists in one slot in which one coil is inserted. It is made of round copper enameled wires. The number of conductors (i.e voltage drops) is selected to be 6. The filling factor, i.e the ratio of copper section in the slot over the total slot surface, is selected to be 0.5. The subdivision of the conductors is determined by the wire's dimensions listed in [16] and the filling factor. To favorize heat transfer, the insulation thicknesses are first considered minimal. The wire is a *grade 1* at minimal tolerance given in [16]. The slot insulation total thickness is taken equal to $20\mu m$.
As at a given insulation grade the bigger a wire is, the higher the PDIV level is, the biggest wire section in the catalog compliant with the filling factor criterion is selected.

Table 5. Statorette data recap

Filling factor	0.5
Coil voltage amplitude	1500V
Overshoot	50%
Wire copper radius	2.5mm
Number of conductors	6
Number of wires per conductor	2
Enamel dielectric constant	3.5
Slot insulation total thickness	$20\mu m$
Slot insulation dielectric constant: ε_{layer1} – ε_{layer2}	3.5 – 3.5
Turn to turn estimated PDIV (parametric model)	871V
Turn to slot estimated PDIV (parametric model)	765V

The number of wires per conductors is then known. Let's consider a nominal voltage amplitude of *1500V* at the motorette terminals. To simulate the overshoot presents on a coil terminal in the context of inverter fed motor, an overshoot of 50% of the nominal voltage amplitude is chosen. Moreover, to consider the nonlinear repartition of the voltage front over the whole coil, the overshoot is only applied to the first conductor. For the other conductors, the voltage repartition is selected to be linear. Tab. 5 recaps all the data used.
Fig. 19 presents the initial configuration with minimum insulation material thicknesses. Each circle is the external contour of a wire. The colors indicate the applied voltage on the wire's copper limit. Colored crosses and dotted connected circles markers indicate the presence of turn to slot and turn to turn PD risk zones respectively. In this case, there is turn to turn PD risk between first (red) and second (yellow) conductor. There is turn to slot PD risk with first conductor and third conductor (green). Tab. 6 gives the maximum voltage drops between turn to turn and turn to slot.

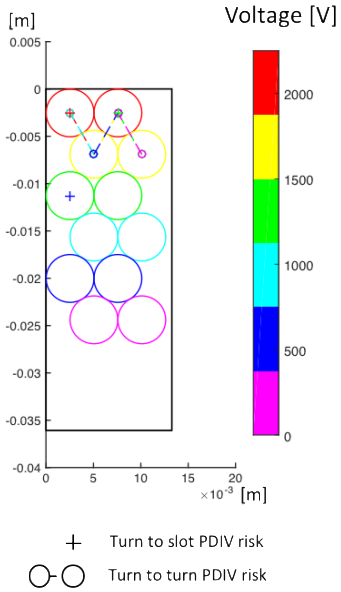

Figure 19. Initial winding configuration in the motorette; turn to turn & turn to slot PD risk

Table 6. Maximum voltage drops in the motorette (initial configuration)

	Maximum voltage drop
Turn to turn	1050V
Turn to slot	2250V

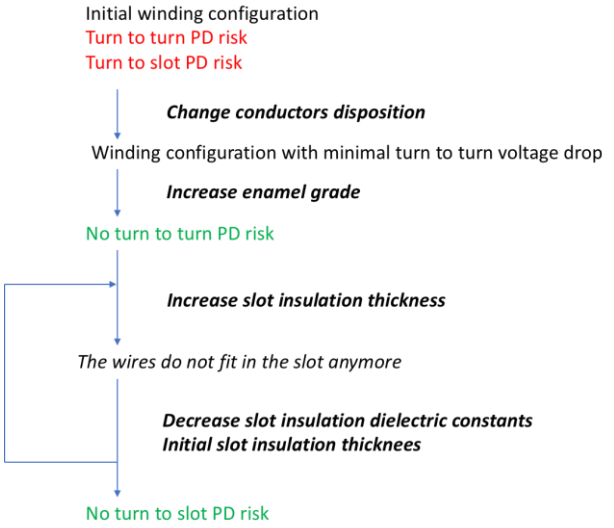

Figure 20: tool simple algorithm

In this example, the enamel dielectric constant value is fixed. The slot insulation is considered to be made of two layers of same thickness. Their dielectric constant can vary. These assumptions reduce the degrees of freedom but also simplify the algorithm for PD risk suppression presented on Fig. 20.
The solution provided by the tool following the presented algorithm is shown on Fig. 21. Tab. 7 recaps the outputs of the solution. The predicted PDIV values are higher than the maximum voltage drops presented on Tab. 6

Table 7. Solution outputs

Wire copper radius	2.5mm
Number of conductors	6
Number of wires per conductor	2
Enamel dielectric constant	3.5
Enamel thickness	46.5 μm
Slot insulation total thickness	270μm
Slot insulation dielectric constant: $\varepsilon_{layer1} - \varepsilon_{layer2}$	3.5 – 2.3
Turn to turn PDIV	1143V
Turn to slot PDIV	2254V

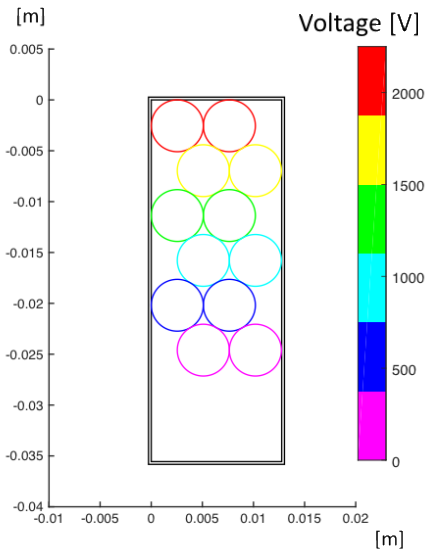

Figure 21. PD free solution

The estimated PDIV values for both the initial and solution configurations are confronted to the ones obtained with the 2D finite elements reduced models (cf Fig. 5). The comparison is shown on Tab. 8.
The obtained error can be explained by the initial dispersion of the data used in the computation of the parametric models. Moreover, the consecutive approximations for the determination of the successive coefficients are also responsible for the error.

Table 8. Comparison of the estimated PDIV values with reduced finite elements models

		Parametric model	2D FE model	Error %
Initial configuration	Turn to turn PDIV	871V	801V	9%
	Turn to slot PDIV	765V	765V	0%
PD free solution	Turn to turn PDIV	1143V	1023V	12%
	Turn to slot PDIV	2254V	2104	7%

9. Conclusion

In this work, parametric models for estimating the PDIV level of turn to turn and turn to slot configurations are presented. There are based on 2D finite elements reduced models results. Successive interpolations using simple mathematic laws are done. The obtained parametric models are confronted to a simple analytical model to check the good evolution of the laws and the orders of magnitude.
The use of such parametric models in a tool to help a machine designer to consider PD risk in the design step is illustrated. The example considers a motorette filled with one coil made of 6 conductors. From an initial configuration where multiple PD risk zones are identified, the tool provided a solution without running any finite elements simulation. The estimated PDIV are then confronted to 2D finite elements simple models. There is a maximum of *12%* error of the estimated values.
In future work, the dielectric constant of the enamel overcoating the wire will be unlocked as a degree of freedom. Attention will be given to the electric field intensity in dielectrics, especially the ones with low dielectric constants values, to ensure that the insulation layer does not reach its electric breakdown level.

10. Acknowledgment

This project has received funding from the Clean Sky 2 Joint Undertaking under the European Union's Horizon 2020 research and innovation program under grant agreement No 715483.

11. References

[1] J. Robinson, 'Collins Aerospace building $67M electric aircraft lab', *Wings Mag.*, Apr. 2019.

[2] 'Hybrid Aircraft Academic reSearch on Thermal & Electrical Components and Systems (HASTECS), Project selected from CFP in Cleansky II (H2020) framework'. .

[3] B. Sarlioglu and C. T. Morris, 'More Electric Aircraft: Review, Challenges, and Opportunities for Commercial Transport Aircraft', *IEEE Trans. Transp. Electrification*, vol. 1, no. 1, pp. 54–64, Jun. 2015, doi: 10.1109/TTE.2015.2426499.

[4] M. Pettes-Duler, X. Roboam, and B. Sareni, 'Integrated design process and sensitivity analysis of a hybrid electric propulsion system for future aircraft', in *Electrimacs 2019*, Salerno, Italy, 2019.

[5] P. Collin, S. Touhami, D. Malec, Y. Lefevre, and J. F. Llibre, 'Design of Electric Machine Taking Into Account the Partial Discharges Phenomena for Future Hybrid Propelled Aircrafts', in *e Proceedings of More Electric Aircraft - MEA 2019*, 2019.

[6] A. Zeaiter and M. Fenot, 'Thermal Sensitivity Analysis of a High Power Density Electric Motor for Aeronautical Application', in *2018 IEEE International Conference on Electrical Systems for Aircraft, Railway, Ship Propulsion and Road Vehicles & International Transportation Electrification Conference (ESARS-ITEC)*, Nottingham, 2018, pp. 1–6, doi: 10.1109/ESARS-ITEC.2018.8607393.

[7] R. Hemmati, F. Wu, and A. El-Refaie, 'Survey of Insulation Systems in Electrical Machines', in *2019 IEEE International Electric Machines & Drives Conference (IEMDC)*, San Diego, CA, USA, 2019, pp. 2069–2076

[8] 'EIC 60034-18-41, "Partial discharge free electrical insulation systems (Type I) used in rotating electrical machines fed from voltage converters – Qualification and quality control tests," 2014.'

[9] J. Pyrhonen, T. Jokinen, and V. Hrabovcová, *Design of rotating electrical machines*. Chichester, West Sussex, United Kingdom ; Hoboken, NJ: Wiley, 2008.

[10] J. Moeneclaey, 'Méthode de conception des bobinages des actionneurs électriques adaptés aux nouvelles contraintes de l'avionique', University of Artois, Béthune, 2015.

[11] L. Benmamas, 'Méthodes d'évaluation du risque de décharges partielles dans le bobinage de machines électriques destinées à la traction automobile', University of Paris-Saclay, Gif-sur-Yvette, 2017.

[12] G. Parent, M. Rossi, S. Duchesne, and P. Dular, 'Determination of Partial Discharge Inception Voltage and Location of Partial Discharges by Means of Paschen's Theory and FEM', *IEEE Trans. Magn.*, vol. 55, no. 6, pp. 1–4, Jun. 2019, doi: 10.1109/TMAG.2019.2902374.

[13] A.-M. Pointu, J. Perrin, and J. Jolly, 'Plasmas froids de décharge - Propriétés électriques', *Tech. Ing.*, no. D2830 V1, p. 26, 1998.

[14] P. Collin, D. Malec, and Y. Lefevre, 'About the relevance of using Paschen's criterion for partial discharges inception voltage estimation when designing the electrical insulation system of inverter fed motors', *Electrical Insulation Conference (EIC)*, Calgary, Alberta (CANADA), 16-Jun-2019.

[15] E. SILI, 'Etude et caractérisation des décharges partielles et du vieillissement du polyimide en environnement aéronautique', Toulouse 3 Paul Sabatier, 2012.

[16] 'enamlled_copper_wire.pdf'. [Online]. Available:http://www.universalmetals.com.pk/pdf/enamlled_copper_wire.pdf. [Accessed: 15-Jan-2020].